

# Humanoid push recovery using sensory reweighting



Noel Maalouf<sup>a,\*</sup>, Imad H. Elhadj<sup>a</sup>, Elie Shamma<sup>b</sup>, Daniel Asmar<sup>b</sup>

<sup>a</sup> Electrical and Computer Engineering, American University of Beirut, Beirut, 11-0236, Lebanon

<sup>b</sup> Mechanical Engineering, American University of Beirut, Lebanon

## ARTICLE INFO

### Article history:

Available online 6 May 2017

### Keywords:

Humanoid fall avoidance  
Sensory reweighting

## ABSTRACT

In this paper we propose a novel system that uses sensory input from both vision and inertial sensors for an improved perception of the robot current status of equilibrium. We use MonoSLAM vision odometry as a basis for the visual perception and a gyro for angular velocity measurements; and we devise a reweighting method within a Kalman filter framework. Moreover, our approach is designed to be robust against visual and measurement noise such as blur, poor lighting conditions, and faulty sensory output. The novelty in this work is a robust humanoid fall avoidance system, which relies on the fusion of sensory input, mainly gyroscope and visual odometry, taking into account changes in the environment. The fusion of the mentioned sensors in addition to the image quality assessment, ensure a more human-like fall avoidance in comparison to currently existing systems. We implement our method on the NAO humanoid, where seven sets of experiments are performed to assess the effectiveness of our approach. The fusion of camera and gyro information not only enables a more human-like behavior, but also provides more humanoid stability and faster recovery, and thus leads to more robust fall avoidance.

© 2017 Elsevier B.V. All rights reserved.

## 1. Introduction

Humanoid fall avoidance is important since it protects the robot against breakage and reduces time needed to recover from a fall. Humanoids are prone to various disturbances that could be harmful if not mitigated properly, especially that humanoids are meant to operate around humans, so bumps and trips are inevitable [1,2]. If no fall avoidance methods are applied, there exists a risk of harm to the individuals in the environment and damage to the robot thus requiring costly maintenance. Most fall avoidance strategies rely on one type of sensors that measure angular position or velocity of the robot's Center of Mass (CoM) [3,4]. However, in everyday operations, these sensors are prone to noise that render the measurements inaccurate and deceptive. For example, if the robot is standing on an uneven terrain, the proprioceptive sensor alone does not give a reliable evaluation of balance. Similarly, gyros and accelerometers are affected by noise which distorts their measurements. In order to ensure robust balance control, this paper integrates a new source of sensory information, that of vision, in addition to the gyro and uses a Kalman filter to fuse the sensory information. As a result, the fusion of visual (camera) and vestibular (inertial) sensory modalities leads to a superior fall avoidance mechanism.

Our approach is bio-mimetic in nature, in fact, humans possess superior balance capabilities and mimicking them would hopefully

help devise a more robust fall avoidance system. During quiet standing, humans tend to rely on three sensor information: visual sensors, vestibular sensors (otolith and semi-circular canals), and somatosensory information (coming from muscles and joints) [5].

Vision plays an important role in human balance recovery, while it contributes to approximately 10% of the control it is found to be the most critical in the decision making [6]. Vision describes the relative motion to the environment [5]. The brain processes visual information in order to differentiate between ego-motion and object motion in the environment. The vestibular system is reported to contribute 20% of the human balance control [7], sensing both angular velocity and linear acceleration of the head [8]. The angular velocity is provided by semi-circular canals, while the otolith organs measure the linear acceleration. Both of these organs lie in the human's inner ear. The vestibular system can be thought of as a level sensor; as the sensor is tilted the fluid inside the sensor (inside the ear for a human) reaches its edge, thereby triggering a feeling that one is falling. As for the somatosensory or proprioceptive information, it includes joint positions as well as muscle activity which are valid indicators of the human posture [9]. This system contributes to 70% of the posture control since it needs the least processing.

After assessing their posture, humans apply three main strategies to overcome external disturbances. The first strategy that humans follow is the ankle strategy [10]. Torque is applied at the ankle joints opposite to the direction of the disturbance. When the magnitude of the disturbance grows, the ankle strategy is no longer

\* Corresponding author.

E-mail address: [njm12@mail.aub.edu](mailto:njm12@mail.aub.edu) (N. Maalouf).

capable of preventing a fall and humans tend to apply the hip strategy, where the hip rotates along the direction of the disturbance in such a manner to absorb the disturbance, then it stops and returns to the equilibrium position using the hip and ankles [11]. When subjected to yet a higher magnitude disturbance, it is only through stepping that humans can avoid falling. This may be accomplished by taking one or more steps depending on the magnitude of the disturbance. A demonstration of the three aforementioned strategies is shown in Figs. 1–3. In humanoid fall avoidance, the stepping strategy is usually considered as a last resort when the ankle and hip are no longer sufficient. However, humans deal with this problem in a different way. Evidence from the literature in Kinesiology [12] indicates that humans tend to take a step way before the magnitude of the disturbance reaches the ankle and hip thresholds. The key difference lies in the information processing and decision making strategies that the human body uses to keep its balance.

When studying human posture, Kinesiologists differentiate between ideal posture and normal posture [13]. Ideal posture requires the least amount of muscular support and minimizes the stresses on the joints. In other words, it is a hypothetical term that represents the posture which minimizes the loads in the supporting ligaments [13]. Normal posture however, presents the actual joint angles and torques that result from extensive experiments on human subjects with no impairments. The experiments focus on the Line of Gravity, which is the vertical projection of the Center of Gravity [14]. Experiments show that during quiet standing, the Line of Gravity must lie within the border of the supporting feet in order to maintain equilibrium. Therefore, the ideal posture is when the Line of Gravity passes through the axes of rotation of the related joints [14]. However, in reality there is no perfect posture, so the Line of Gravity tends to pass anteriorly or posteriorly to the affected joint axes. This is the normal posture. As the distance separating the Line of Gravity from the joint axis increases, the gravitational moment increases, and thus a counter torque is needed to decrease the distance [14].

Most humanoid balance systems to date focus on Zero Moment Point (ZMP) control [15]. ZMP is the contact point of the foot with the ground where the sum of the inertial and gravity forces is zero [16]. This concept also applies to human behavior, however the difference lies in how posture is sensed. Few attempts have been made to take measurement noise into consideration while assessing balance. Mahboobin et al. [17] introduced a sensory reweighting mechanism in order to fuse vestibular and proprioceptive information. The reweighting scheme consists of two Kalman filters, each giving more preference to one sensor over the other (through Kalman gain changing). Another work on sensory reweighting in humanoid fall avoidance involves the fusion of the gyro and accelerometer sensors which together constitute the vestibular system [8]. However, none of the previously mentioned systems includes vision. In fact, the first system that applies sensory reweighting of visual, vestibular and proprioceptive information was recently introduced by Klein et al. [18]. The visual information is obtained from optical flow analysis, while an adaptive Kalman filter calculates three gains depending on the noise covariance of each sensor [18]. Although vision is included in posture estimation, its role is limited to the distance separating the robot from the visual environment. Any change in this distance causes inaccurate posture estimation and thus a faulty control strategy. So, the system only functions in a predetermined environment. Another limitation lies in the fact that the system is not designed to cope with unpredicted visual changes such as blurriness or poor lighting conditions. Therefore, our aim is to integrate a better visual estimation technique (MonoSLAM) and account for environmental changes such as blurry scenes and poorly lit areas. This enables better humanoid pose estimation and push recovery in scenarios

where the previously mentioned algorithms fail. Another approach that uses vision but without sensory reweighting is introduced by Mahani et al. [19], where stereovision is used to estimate the humanoid's Center of Mass pose and the knee/knee–hip strategies are used for push recovery. This approach fully relies on vision, which makes it non-reliable in poor lighting conditions and in environments with blurry scenes.

The sensory reweighting systems mentioned above are all tested for small-angle swaying disturbances applied to the platform on which the humanoid is standing on. However, push disturbances differ from pure swaying in their magnitude and impulse-like behavior. In our system, the fall avoidance strategy is tested by applying a push force to the humanoid robot and recording its response in terms of ankle torques in addition to the swaying angles.

The contributions of this paper are threefold. First, it integrates the use of Visual MonoSLAM and gyroscope measurements for better humanoid pose estimation. This helps in overcoming the limitation of a predetermined distance between the humanoid and the visual scene. While the integration of Visual MonoSLAM has been widely used in the literature as in [20], to the best of our knowledge it has not been used in humanoid posture assessment. Second, the blur and brightness factors are introduced to better assess the quality of the acquired visual pose estimation. These factors are used to decide the degree of reliance on each of the camera and the gyroscope information. Third, the system is tested against push disturbances which are of higher magnitudes than the swaying disturbances applied on other systems. It is important to note that the novelty is not in the Kalman Filter used for the fusion, but in the use of fusion for humanoid push recovery in addition to analyzing the visual scene quality and integrating it in the fusion. Therefore, other methods could also be used for fusion but the key is mimicking the human behavior of relying on multiple sensor inputs and adding a reliable assessment of the visual information by integrating blur and brightness metrics. In addition, the fusion technique introduced in this paper can be used to enhance any existing fall avoidance control strategy which takes the posture's angle and angular velocity as inputs.

The rest of the paper is organized as follows. Section 2 reviews the background related to humanoid fall avoidance and its relevance to human fall avoidance strategies. The robot model and the control strategy are covered in Section 3. Section 4 explains the Visual SLAM method used to estimate humanoid posture, while Section 5 introduces the sensory reweighting system. An overview of the humanoid robot used as well as the experimental setup is presented in Section 6. Section 7 shows the experimental results followed by a thorough analysis. The conclusion is stated in Section 8, while the discussion and future work are stated in Section 9.

## 2. Background on humanoid/human fall avoidance

Humanoid stance and gait balance has been the subject of many research projects since the early 1980s. In 1984, Ichiro Kato applied the Zero Moment Point (ZMP) concept to balance a biped's gait [16]. In fact, this achievement came more than a decade after the introduction of the ZMP concept. This concept is considered as one of the basics of bipedal balance and is still applied today to maintain posture stability in humanoids.

In short, the ZMP is defined as the point (on a supporting surface) at which the sum of moments of inertial and gravity forces is zero along a horizontal axis. However, if the calculated point lies outside the support polygon, it is then called Fictitious ZMP. As a result, the humanoid needs to take one or more steps to regain equilibrium [16].

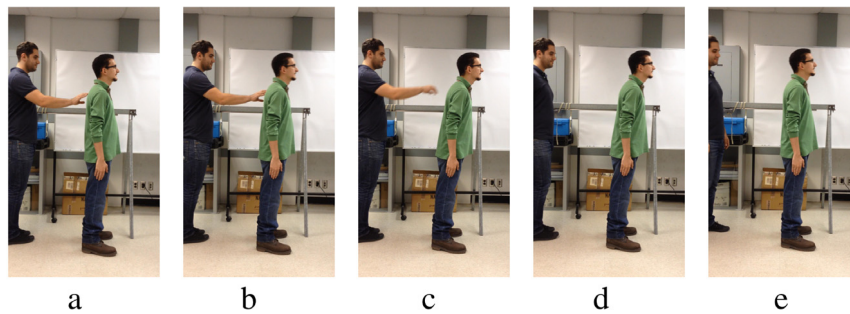


Fig. 1. Demonstration of the ankle strategy.

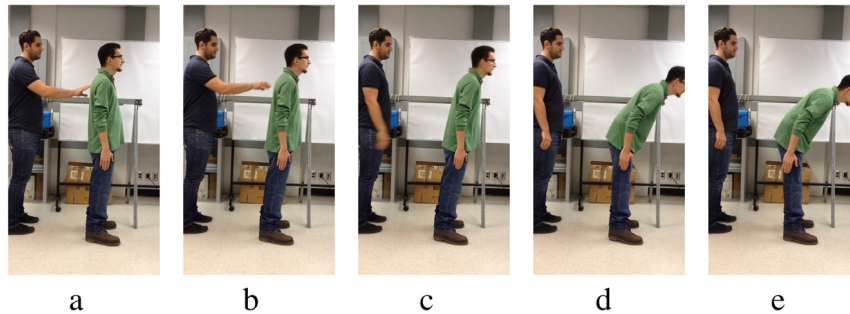


Fig. 2. Demonstration of the hip strategy.

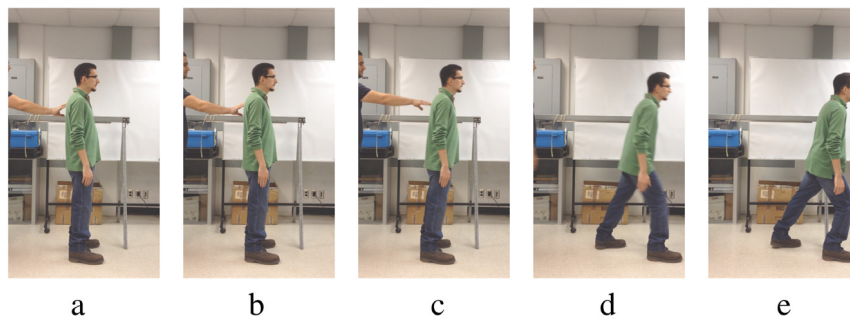


Fig. 3. Demonstration of the stepping strategy.

### 2.1. Existing systems

The attempts for achieving postural balance have started by modeling the humanoid as a mechanical system and trying to control its balance. Some work aims at finding the best robot-joint material that has the right compliance to compensate for external disturbances [21]. A recent compliant humanoid is COMAN [21], a humanoid that has elastic transmission in its joints allowing smoother response to disturbances. Instead of mimicking the human joint structure, some researchers resort to learning methods based on human behavior to maintain humanoid quiet standing balance as in [22].

Many researchers focused on applying the ankle, hip and stepping strategies for maintaining balance. Jalgha et al. [3] developed a decision surface between the ankle and hip strategies in the sagittal plane. The decision is based on initial inclination angle and angular rotation velocity after the push disturbance is applied. Humanoid quiet stance could also be maintained using Capture Points. This method is developed by Pratt et al. [23]. The algorithm is based on the ZMP and fictitious ZMP which were discussed earlier. Capture points can be applied for disturbances in differently-oriented directions but its complexity lies in the modeling process of the humanoid and in the control of the stepping action when applied.

For small disturbances, the ankle strategy alone is enough to recover, while for larger disturbances, a combination of both ankle and hip strategies is needed to overcome the push.

In the above work, the main focus is on the recovering behavior of the humanoid robot. This of course is essential, but it overlooks an important role which is the robust and accurate assessment of the posture stance. What is meant by robust and accurate is a human-like use of vision and gyro in push recovery.

Humans have superior balance strategies to prevent falling, so it might be intuitive to try to mimic human behavior in humanoid fall avoidance. The human sensory system is complex and in order to sense posture it takes recourse to its visual, vestibular, and somatosensory subsystems. Humanoid robots are usually equipped with sensors similar to those of humans [7]. In most fall avoidance strategies, the vestibular system is imitated by using a gyroscope; a sensor which measures postural angular velocity as the inner ear does in the human body. The somatosensory system which is responsible for measuring contact forces is imitated by using force sensors such as Force Sensitive Resistors (FSR). However vision, which plays a very important role in human balance control, is rarely used for humanoid stability. In fact, systems that include vision utilize it within very constrained environments and extract limited information from it [18].

Vision dominates pose estimation in well-lit and clear environments [7]. Experiments have shown that blind subjects experience poorer postural control than sighted subjects, which indicates the importance of vision [24]. In addition to pose estimation, vision is critical for obstacle avoidance and environment assessment.

On the other hand, every sensor no matter how essential in pose estimation is susceptible to noise. Examples of noise applied to human vision include dark environments, blurry scenes, or simply a moving environment while the subject is standing still [7]. In such situations, the human brain dedicates more weight to the information received from vestibular and somatosensory systems. For example, when subjects were placed in a rotating room they were deceived for a short period of time since the visual system was providing false information to the brain. However, when less weight was given to vision, the subject's postural control returned to its normal state and balance was achieved again [7].

In humanoids, as in all sensory systems, the sensors used are always susceptible to noise and therefore one cannot rely on a single sensor to cover all situations. We choose to implement sensor integration in order to diminish the effect of noise. Sensory integration ensures successful operation of the humanoid fall avoidance system in a wider range of environments under various conditions. It is important to note again that this paper's contribution is improving the humanoid's push recovery by integrating camera and gyroscope information and assessing the visual scene. The aim is not to introduce a new recovery strategy. Moreover, the integration of visual MonoSLAM with other sensors has been done in the literature. For example in [20] and [25], the fusion of IMU and MonoSLAM readings enables depth (scale) estimation. In our work, the sensory integration is utilized in the balancing of the humanoid under varying conditions.

The state estimation approach is sometimes used for dealing with unknown modeling errors as in [26]. Xinjilefu et al. compare state estimation techniques for better humanoid walking strategies [27]. State estimation can also be used to detect and correct drifts in the humanoid's path following task as in [28,29]. In [28], the algorithm uses inertial, kinematic, and LIDAR information to estimate the humanoid's position.

### 3. Robot model and torque control

In this section, we propose a model to capture the stance of the humanoid, state our assumptions, and introduce the control strategy.

#### 3.1. Robot model

In this paper, we limit our analysis to the fall avoidance in the sagittal plane alone, accordingly, we model the humanoid as an inverted pendulum where the angle difference at the ankles is the control input and the ankle torque is the output. The robot model is shown in Fig. 4, where CoM is the humanoid's Center of Mass,  $a$  is the angular displacement of the ankle,  $L_0$  is the distance from the foot to the ankle,  $L_L$  is the distance from the ankle joint to the CoM,  $D^+$  is the distance from the foot base to the front tip, while  $D^-$  is the distance from the foot base to the foot's rear end, and  $\beta$  is the foot rotation angle.

In order to model the humanoid as a linear inverted pendulum, the following assumptions are made:

- The body is considered as a point mass located at the humanoid's center of mass (CoM).
- The humanoid's foot rotation angle with respect to the ground is  $\beta$ .
- The length from the humanoid's feet to its CoM is constant.
- The hip and knees are locked and the only torque applied is at the ankles.

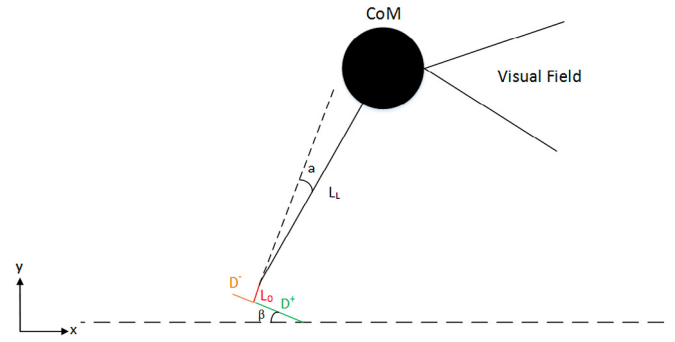


Fig. 4. Humanoid robot modeled as a Linear Inverted Pendulum.

Table 1

VMC parameters and their significance.

$\beta$	Humanoid foot rotation angle
$a$	Displacement angle at the ankles
$D^+$	Distance between ankle and front tip of the foot
$D^-$	Distance between ankle and back of the foot
$L_0$	Distance between foot and ankle actuator
$L_L$	Distance between ankle actuator and CoM
$F_S$	Spring force
$F_D$	Dashpot force
$F_Y$	Vertical force opposite to the gravitational force
$K$	Spring constant
$B$	Damping constant
$L_C$	$L_0 + L_L$

#### 3.2. Torque control

The ankle strategy implemented on the humanoid is inspired by Jalgha et al. [3] whose work is an extension of the ankle strategy developed by Stephens [30]. The aim of our work is to improve the ankle strategy by following a more human-like assessment of the humanoid posture through sensor fusion. The control algorithm is that of a Virtual Model Control (VMC) which is based on attaching virtual components to a robot in order to control its behavior. The forces created by these mechanical components affect the torques applied on the corresponding actuators and in turn control the robot's movements. The VMC implemented on our humanoid consists of a virtual spring and dashpot system (connected in parallel) attached to the humanoid's CoM on one side and to a roller on the other. The parameters discussed in this section are defined in Table 1.

The transformation matrix that relates the world frame to the CoM frame of the humanoid is shown in (1), where  $D$  is either  $D^+$ , 0, or  $D^-$  depending on the position of the humanoid's foot [3]:

$$\mathbf{T} = \begin{pmatrix} s_{\beta+a} & -c_{\beta+a} & 0 & D - (Dc_{\beta} + L_0s_{\beta} + L_Ls_{\beta+a}) \\ -c_{\beta+a} & -s_{\beta+a} & 0 & -Ds_{\beta} + L_0s_{\beta} + L_Lc_{\beta+a} \\ 0 & 0 & -1 & 0 \\ 0 & 0 & 0 & 1 \end{pmatrix}. \quad (1)$$

Since the humanoid is modeled as a linear inverted pendulum, a single inclination angle ( $\theta$ ) is considered which is the inclination of the CoM from the vertical line. The work is focused on the robot's motion in the sagittal plane, so  $\theta$  could be derived from the  $x$ - $y$  position of the robot's CoM taken from the last column of  $\mathbf{T}$  in (1):

$$\theta = \arctan \frac{x}{y} = \arctan \frac{D - (Dc_{\beta} + L_0s_{\beta} + L_Ls_{\beta+a})}{-Ds_{\beta} + L_0s_{\beta} + L_Lc_{\beta+a}}. \quad (2)$$

The Jacobian relating the joint torques to the virtual forces is found in (3):

$$\mathbf{J} = \begin{pmatrix} \delta x / \delta a \\ \delta y / \delta a \end{pmatrix} = \begin{pmatrix} -L_L c_{a+\beta} \\ -L_L s_{a+\beta} \end{pmatrix}. \quad (3)$$

The virtual forces  $F_S$ ,  $F_D$ , and  $F_Y$  are expressed in (4):

$$\begin{aligned} F_S &= Kx = K(D - (Dc_\beta + L_0s_\beta + L_Ls_{\beta+a})) \\ F_D &= B\dot{x} = B(\dot{\beta}(Ds_\beta - L_0c_\beta) - (\dot{a} + \dot{\beta})L_Lc_{\beta+a}) \\ F_X &= F_S + F_D \\ F_Y &= mg \\ \mathbf{F} &= \begin{pmatrix} F_X \\ F_Y \end{pmatrix}. \end{aligned} \quad (4)$$

The virtual spring and damper forces represented by  $F_S$  and  $F_D$  respectively act in the  $x$ -direction and are summed up in  $F_X$ , while  $F_Y$  is used to cancel the effect of gravity. The torque applied at the ankle joints is calculated using the Jacobian property where the actuator torque is the product of the transpose Jacobian and the forces acting on the end effector, being the humanoid's center of mass in this case.

$$\tau = \mathbf{J}^T \mathbf{F} = -F_X(L_Lc_{a+\beta}) - F_Y(L_Ls_{a+\beta}) \quad (5)$$

The torque in (5) is passed to the ankle joints to maintain stability:

#### 4. Pose estimation using Monocular SLAM

In order to acquire visual information, we use a single camera and apply a Monocular SLAM (Simultaneous Localization and Mapping) algorithm developed by Davison et al. [31] in order to estimate the robot pose and angular velocity. The MonoSLAM algorithm consists of selecting landmarks from the visual scene of the robot and extracting features in the image. Tracking these features during camera movement, allows for motion estimation. The feature position and orientation estimation is calculated through an Extended Kalman Filter [31]. The feature detection is based on 1-point RANSAC (Random Sample Consensus). The algorithm consists of detecting corners and following their motion between image frames. In addition, the uncertainty surrounding each estimated point is calculated and considered when solving for the new state. According to [31], the camera state vector ( $\mathbf{x}$ ) is:

$$\mathbf{x} = [\mathbf{r} \ \mathbf{q} \ \mathbf{v} \ \omega] \quad (6)$$

where  $\mathbf{r}$  is the orientation vector,  $\mathbf{q}$  is the orientation quaternion,  $\mathbf{v}$  is the velocity vector, and  $\omega$  is the angular velocity. The noise is assumed to be zero-mean Gaussian and applied as an acceleration noise. This leads to an impulse change in velocities. The noise vector is shown in (7):

$$\mathbf{n} = [\mathbf{n}_{\text{linear}} \ \mathbf{n}_{\text{angular}}]^T = [\gamma \Delta t \ \alpha \Delta t] \quad (7)$$

where  $\gamma$  and  $\alpha$  are the unknown linear and angular acceleration respectively. The updated elements of the camera state vector are shown in (8)–(11):

$$\mathbf{r}_{\text{updated}} = \mathbf{r} + (\mathbf{v} + \mathbf{n}_{\text{linear}})\Delta t. \quad (8)$$

$$\mathbf{q}_{\text{updated}} = \mathbf{q} \times \mathbf{q}((\omega + \mathbf{n}_{\text{angular}}))\Delta t \quad (9)$$

$$\mathbf{v}_{\text{updated}} = \mathbf{v} + \mathbf{n}_{\text{linear}} \quad (10)$$

$$\omega_{\text{updated}} = \omega + \mathbf{n}_{\text{angular}}. \quad (11)$$

Using the above values, we deduce the robot's change in angular position and velocity in order to estimate its posture. Therefore, we are able to use vision as a position and velocity estimator independent of the environment in which the robot is operating. It is important to note that poor lighting conditions and blurriness will affect the estimation. However, those two factors are taken into consideration in the final system, which is discussed in Section 5.

The MonoSLAM code returns the robot's state as a quaternion; however in our case we only need the humanoid's pitch angle since

we are working in the sagittal plane. Given a rotation matrix  $\mathbf{R}$ , the pitch angle ( $\theta$ ) in radians is calculated using (12) [31]:

$$\theta = \arctan \frac{-\mathbf{R}(2, 0)}{\sqrt{\mathbf{R}^2(2, 1) + \mathbf{R}^2(2, 2)}}. \quad (12)$$

While visual feedback enhances the fall avoidance strategy, the quality of the acquired images has an effect on the pose estimation. For this reason it is important to take image quality into consideration. Two metrics are assessed at each frame and their values affect the error covariance of the Kalman Filter. The blur metric is calculated by blurring the image both horizontally and vertically followed by calculating the difference between the blurred image and the original one [32]. The horizontal and vertical filters used to blur the image frames are shown in (13). The idea behind this algorithm is that if we start with a blurry image, adding blurriness will not have a difference between the original and the updated one [32]. This way we can determine the blur factor of the visual scene. The blur metric is a value between 0 and 1, where 0 indicates a perfectly sharp image and 1 indicates a fully blurred image [32].

Another important factor that affects image quality is the brightness metric. This is analogical to the human case where the dependency on vision decreases in dark environments. The brightness is calculated by taking the mean of the *Value* matrix<sup>1</sup> of the image in HSV (Hue–Saturation–Value) format. The brightness metric is also normalized where 0 means totally dark and 1 means fully bright. The desired blur factor is a value close to 0, while the optimum brightness factor is around 0.5 (midway):

$$H_{\text{hor}} = 1/9(1 \ 1 \ 1 \ 1 \ 1 \ 1 \ 1 \ 1 \ 1) \quad H_{\text{ver}} = H_{\text{hor}}^T. \quad (13)$$

#### 5. Sensory reweighting system

The overall system consists of three main blocks; robot angle and angular rate estimation (using vision and gyroscope), Kalman filter, and torque controller (see Fig. 5). The vision pose estimation was discussed in the previous section and the angular velocity is directly measured using the gyroscope of the NAO humanoid robot.

##### 5.1. Kalman filter

The Kalman Filter is used to fuse the camera and gyroscope measurements and come up with a better estimate of the humanoid's pose. The state space model of the system is presented in (14):

$$\begin{aligned} \mathbf{x}_n &= \mathbf{A}\mathbf{x}_{n-1} + \mathbf{B}\mathbf{u}_n + \omega_n \\ \mathbf{y}_n &= \mathbf{C}\mathbf{x}_n + v_n \end{aligned} \quad (14)$$

$$\mathbf{x}_n = \begin{pmatrix} \theta \\ \dot{\theta} \end{pmatrix} \quad \mathbf{A} = \begin{pmatrix} 1 & \Delta t \\ \frac{g}{L} & \Delta t \end{pmatrix}$$

$$\mathbf{B} = \begin{pmatrix} 1 \\ \frac{1}{mL^2} \Delta t \end{pmatrix} \quad \mathbf{C} = \begin{pmatrix} 1 & 0 \\ 0 & 1 \end{pmatrix}$$

where  $\mathbf{x}_n$  is the current state vector,  $\mathbf{u}_n$  is the input vector, and  $\mathbf{y}_n$  is the measurement vector. The process and measurement noise vectors are represented by  $w_n$  and  $v_n$  respectively. The process noise covariance matrix ( $\mathbf{Q}$ ) and the measurement noise covariance matrix ( $\mathbf{R}$ ) are shown below:

$$\mathbf{Q} = \begin{pmatrix} 0 & 0 \\ 0 & \sigma_\omega^2 \end{pmatrix} \quad \mathbf{R} = \begin{pmatrix} \sigma_\theta^2 & 0 \\ 0 & \sigma_{\dot{\theta}}^2 \end{pmatrix}.$$

<sup>1</sup> The Value matrix represents the intensity (brightness) of each pixel in the image.

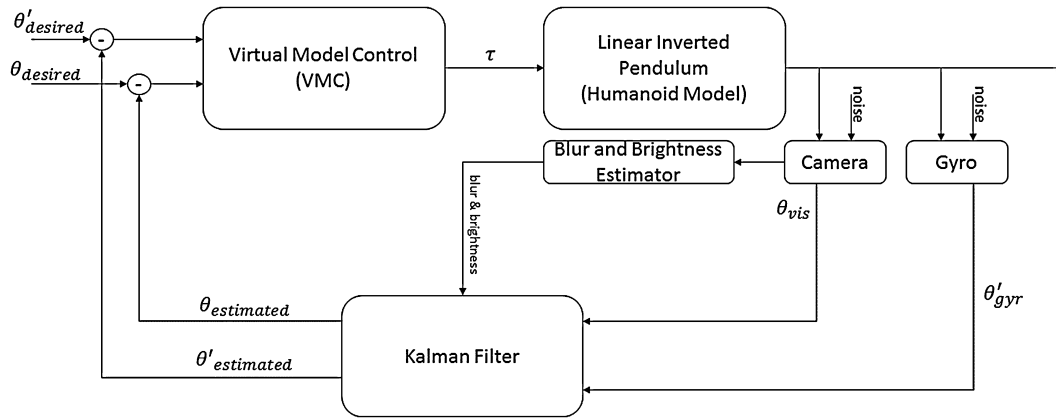


**Fig. 5.** Control Loop of the overall system. The visual and gyro measurements are subjected to noise. The Kalman Filter fuses the measurements along with the blur and brightness metric and sends the predicted angular position and velocity to the Virtual Model Controller which in turn sends the appropriate ankle torque ( $\tau$ ) in order to maintain postural balance.

The process noise standard deviation is  $\sigma_\omega$ , while the visual and gyro measurement noise standard deviations are  $\sigma_\theta$  and  $\sigma_\delta$  respectively. The blur and brightness factors introduced in the previous section, are integrated into the measurement noise covariance update as shown in (15). Since the blur and brightness factors are only related to the visual information, their values are used to update the first element of the measurement noise covariance matrix  $\mathbf{R}$ . The idea behind this equation is that the worse the brightness or the blur metric is the more weight is given to the difference between the old and the new covariance matrices. In the ideal case, where  $bl = 0$  and  $br = 0.5$ , no weight is given to the difference as the measurements are considered to be reliable:

$$\mathbf{R}_n(1, 1) = \mathbf{R}(1, 1) + (bl + |br - 0.5|/2) * (\mathbf{R}(1, 1) - \mathbf{R}_{n-1}(1, 1)). \quad (15)$$

In order to give time for the sensor information to be reliable,  $\mathbf{R}$  is initialized to be  $\mathbf{R}_0 = 5\mathbf{R}$ .

### 6. Experimental setup

The MonoSLAM algorithm is tested alone prior to conducting the seven experiments. The MonoSLAM demonstration is shown in Fig. 6. The four frames are part of a robot's pitch motion from  $0^\circ$  to  $9.4^\circ$  with a velocity of about  $1.5^\circ/s$ . The estimated pitch angle using MonoSLAM was correct to within an error  $0.03^\circ$ .

We can notice in Fig. 6 that in the first frames, few features are detected and most of them represent corners in the scene. The corners are usually the most reliable features in an image, since tracking them is much easier than tracking edges [33]. The humanoid used for experimenting is the Nao H25V3.3, a product of Aldebaran Robotics (see Fig. 7). Nao is 57 cm tall and weighs 5.2 kg. The robot is equipped with a 2-axis gyroscope, which is used to measure the angular velocity. Although NAO is equipped with two cameras, there is no common field of view between them and thus no stereo vision can be done. We also chose to use a Microsoft LifeCam HD (mounted on the head of the robot) in order to get better image quality. The Nao robot does not permit torque control antively, so we opted to use the calculated torque in order to control the ankle motors' stiffness which is feasible on Nao.

The push recovery algorithm is written in C++ running on Ubuntu 12.04. The humanoid robot is set to stand in an upright position with the webcam strapped to its face. The Nao robot is also tied to a linear guide for safety. This guide is frictionless and does not affect the humanoid's movement. It only protects the robot in case the fall avoidance algorithm fails.

In order to get a consistent push force for all trials the humanoid is hit by a ball hanging from a rope and released at a predetermined angle. The experimental parameters are listed below.

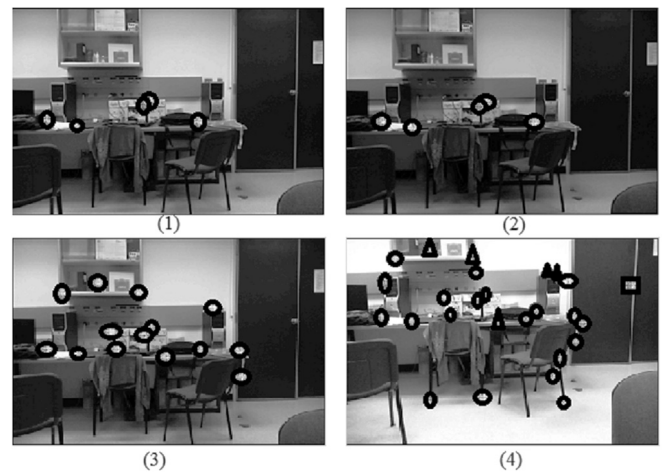


**Fig. 6.** Frames from a camera with MonoSLAM run on MATLAB. The detected features increase with the number of frames; however some of the new features are not very certain (triangles and squares).

- Rope length is 76 cm.
- Distance between robot's back and projection of the ball is 40 cm.
- Height at rest (between bottom of the ball and ground) is 23 cm.
- Angle of release (with respect to the normal) is  $45^\circ$ .
- Ball weight is 425.85 g.
- Ball diameter is 21.804 cm.

After 100 trials using the above mentioned setup, the average force(measured using a force sensor) at the back of the NAO robot is 56.095 N with a standard deviation of 2.697 N. The 95% confidence interval for the applied force is in the range of 52.0 and 61.2 N. The system is shown in Fig. 7.

### 7. Results and analysis

The experiment is conducted in seven different scenarios each repeated ten times, in order to test the robustness and improvement the sensory reweighting gives in push recovery. The scenarios are:

1. Gyro and camera integrated for push recovery under normal conditions.
2. Gyro alone for push recovery under normal conditions.



**Fig. 7.** The whole system is shown in this figure. The humanoid and camera are connected to the laptop running C++ and python code.

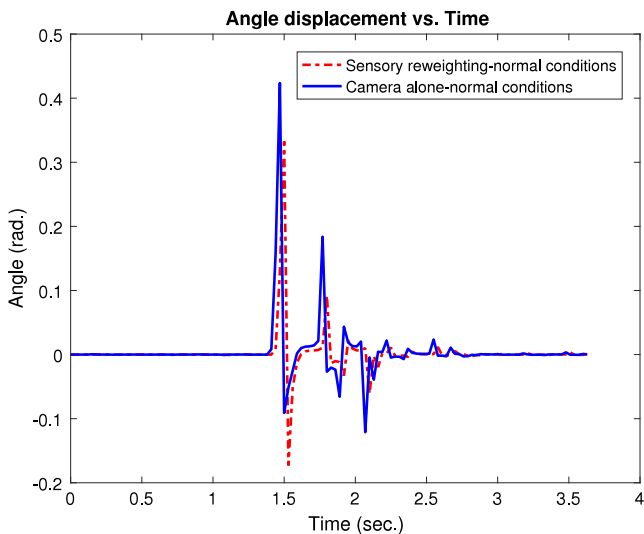


**Fig. 8.** Angle displacement plots using Sensory reweighting (red) and Camera alone (blue) for a 56 N push force under normal conditions. (For interpretation of the references to color in this figure legend, the reader is referred to the web version of this article.)

3. Noisy gyro measurements integrated with camera.
4. Noisy gyro without camera integration (no reweighting).
5. Camera only under normal conditions.
6. Camera and gyro in a dark environment (lights out).
7. Camera only in a dark environment (no reweighting).

The following sections present comparisons between the different scenarios which highlighting the superiority of the sensory reweighting system. The average angle displacements (obtained from Nao's IMU) and ankle torques taken across trials are compared for the seven scenarios. It is important to note that the recovery algorithm is applied on Nao's ankle joints and that all of its other joints are locked. In fact, since the algorithm is only applied in the sagittal plane, only Nao's pitch ankle motors are controlled.

#### 7.1. Sensory reweighting vs vision alone (under normal conditions)

The experiment described above is conducted both when sensory reweighting is applied and when the camera is used alone. The

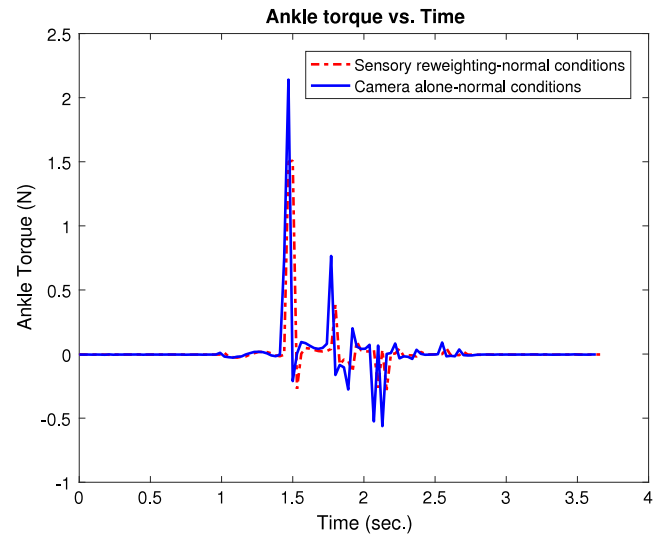


**Fig. 9.** Ankle torque plots using Sensory reweighting (red) and Camera alone (blue) for a 56 N push force under normal conditions. (For interpretation of the references to color in this figure legend, the reader is referred to the web version of this article.)

tests are done under normal conditions. The angle displacement and ankle torque plots are shown in Figs. 8 and 9 respectively. We can notice that sensory reweighting leads to a lower angle displacement (peak of 0.33 rad.) compared to 0.42 rad, when only vision is used. In addition, sensory reweighting improves the settling time by 9.3% (1.17 s compared to 1.29 s). As for the applied ankle torque during the fall avoidance strategy, sensory reweighting requires the application of 1.5 N while vision alone requires a peak of 2.14 N. The results show the superiority of sensory reweighting over using vision alone.

#### 7.2. Sensory reweighting vs gyro alone (under normal conditions)

In this section, the sensory reweighting results are compared to the case where the gyro is used alone. The angle displacement and ankle torque plots are shown in Figs. 10 and 11 respectively. Although using gyro alone leads to a lower angle displacement (peak of 0.17 rad), this method has a poor settling time (1.95 s) compared to the sensory reweighting method. Sensory reweighting is also superior in terms of the maximum applied torque (1.5 N) compared to 3.75 N applied when gyro is used alone. This comparison also indicates the improvement introduced by relying on both gyro and camera measurements.

#### 7.3. Sensory reweighting vs vision alone (lights out)

The sensory reweighting system is tested against a scenario where only the camera is used to estimate the humanoid's posture. This test is performed in a dark environment. The angle displacement and torque plots are shown in Figs. 12 and 13 respectively. It is clear that using a camera alone to assess posture is problematic. This is shown in the angle displacement plot where the estimated angle is zero during to the whole strategy which leads to a negligible torque applied at the ankle joints. As a result, the humanoid is unable to recover from the push and falls down. On the other hand, when sensory reweighting is used, the humanoid relies more on the gyro measurement and is able to successfully recover from the push.

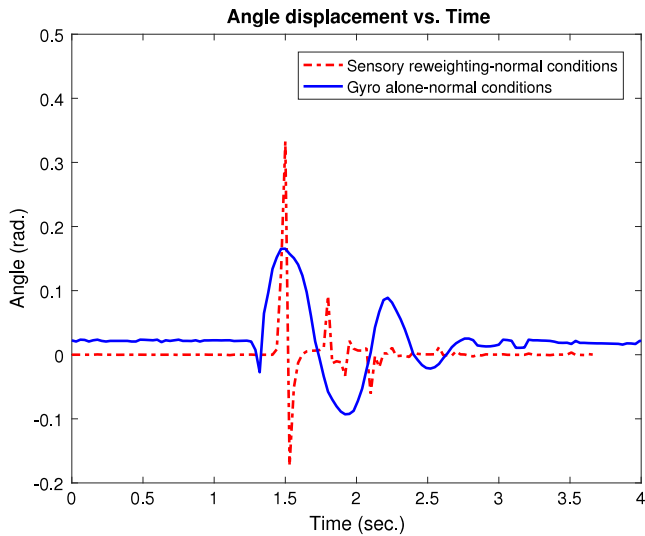


**Fig. 10.** Angle displacement plots using Sensory reweighting (red) and Gyro alone (blue) for a 56 N push force under normal conditions. (For interpretation of the references to color in this figure legend, the reader is referred to the web version of this article.)

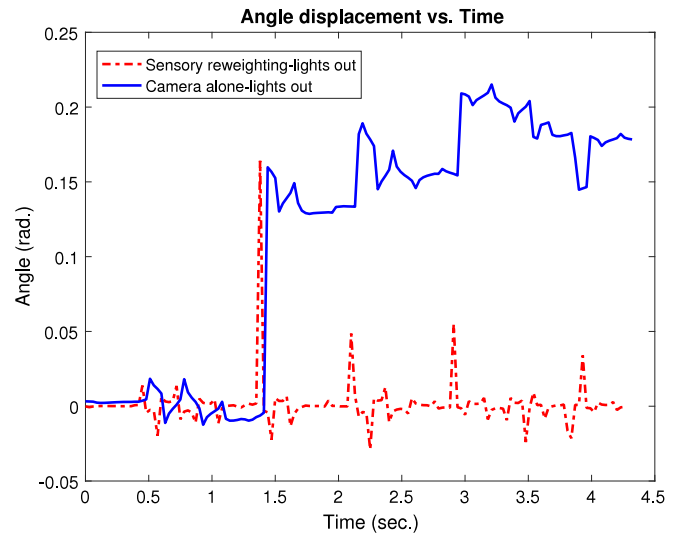


**Fig. 12.** Angle displacement plots using Sensory reweighting (red) and Camera alone (blue) for a 56 N push force in a dark environment. (For interpretation of the references to color in this figure legend, the reader is referred to the web version of this article.)

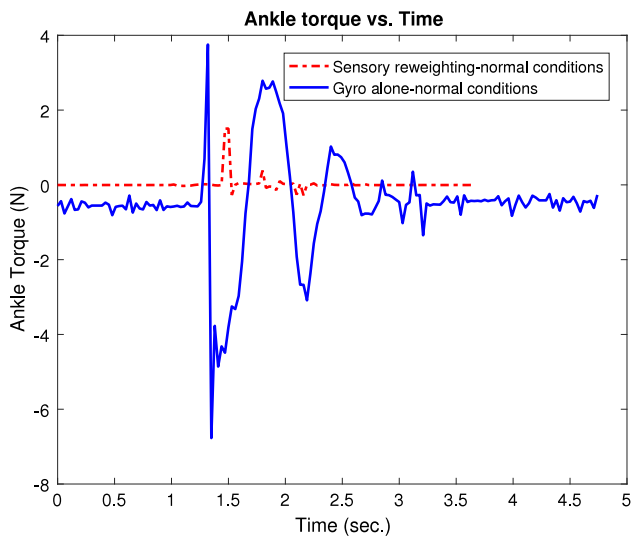


**Fig. 11.** Ankle torque plots using Sensory reweighting (red) and Gyro alone (blue) for a 56 N push force under normal conditions. (For interpretation of the references to color in this figure legend, the reader is referred to the web version of this article.)

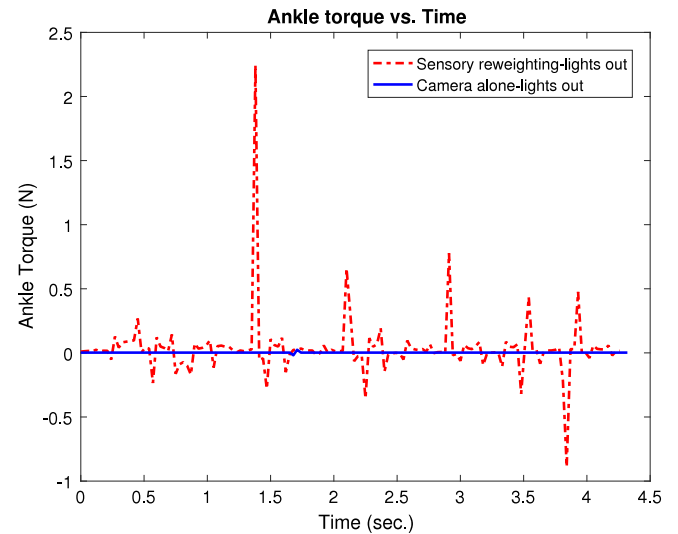


**Fig. 13.** Ankle torque plots using (red) Sensory reweighting and Camera (blue) alone for a 56 N push force in a dark environment. (For interpretation of the references to color in this figure legend, the reader is referred to the web version of this article.)

7.4. Sensory reweighting vs gyro alone (with added gyro noise)

In this comparison, a zero mean Gaussian noise with a unit standard deviation is applied to the gyro measurements and the performance of the sensory reweighting system is tested against a gyro-only system. The angle displacement and torque plots are shown in Figs. 14 and 15 respectively. The sensory reweighting system proves superior in terms of settling time (0.36 s) compared to 1.98 s when using gyro alone. However, the gyro-only method leads to smaller angle displacement (a peak of 0.17 rad) while the sensory reweighting system requires a greater angle (0.39 rad). The sensory reweighting system proves to be more energy efficient since it requires the application of an ankle torque only for a short period of time, while in the gyro-only system a torque is always applied at the ankle joints which might lead to overheating if the strategy is applied for long periods of time. The average values

of the performance parameters (across the 10 repetitions) of the different scenarios are summarized in Table 2.

In order to test the robustness of the sensory reweighting algorithm against gyroscope noise, we also conduct the experiment with double the magnitude of the Gaussian noise added to the gyroscope measurements. Under high magnitude noise sensory reweighting improves the maximum swaying angle by 17.47% and requires less overall torque than when the gyroscope measurements are used alone (see Fig. 16). Despite the fact that when the gyroscope measurements are used alone 60.96% less maximum torque is required to recover, the peak torque is only applied for 0.18 s while ankle torque is always applied in the 'gyro alone' approach (see Fig. 17).

8. Discussion

Sensory reweighting improves fall avoidance in terms of applied ankle torque, angle displacement, and settling time. Referring

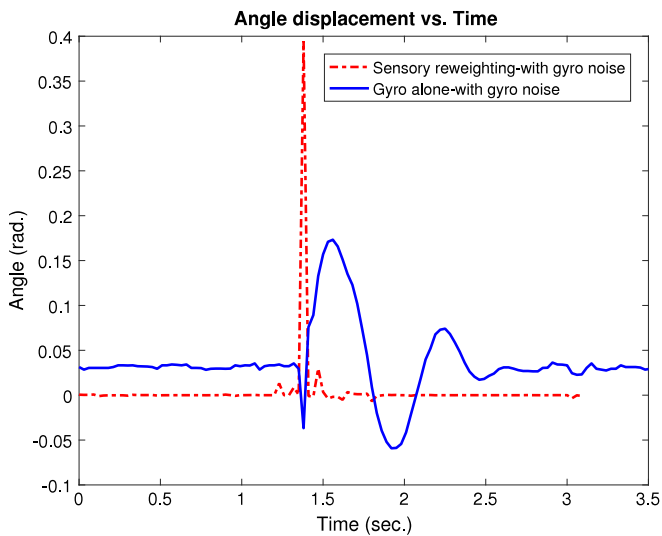


**Fig. 14.** Angle displacement plots using Sensory reweighting (red) and Gyro alone (blue) for a 56 N push force when gyro noise is added. (For interpretation of the references to color in this figure legend, the reader is referred to the web version of this article.)

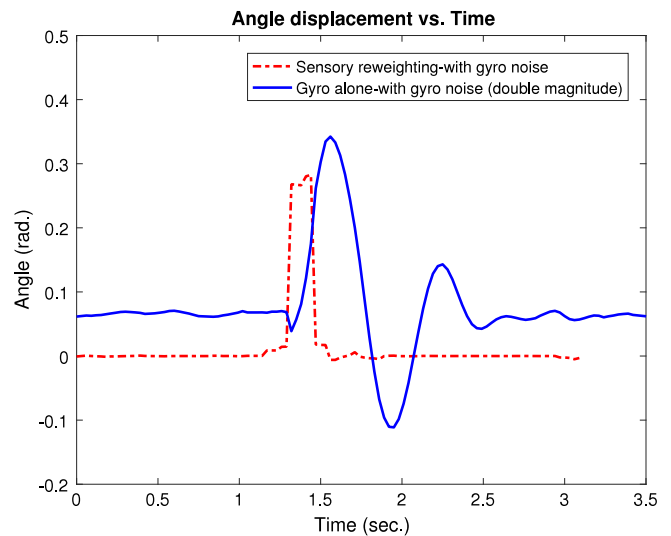


**Fig. 16.** Angle displacement plots using Sensory reweighting (red) and Gyro alone (blue) for a 56 N push force when a double magnitude gyro noise is added. (For interpretation of the references to color in this figure legend, the reader is referred to the web version of this article.)

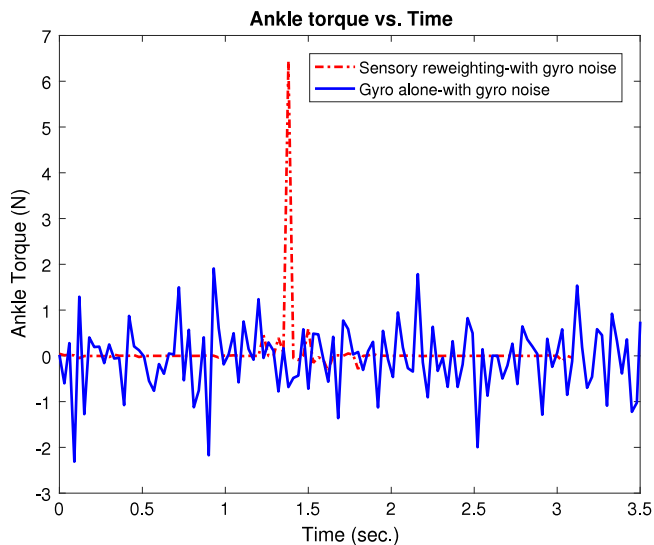


**Fig. 15.** Ankle torque plots using Sensory reweighting (red) and Gyro alone (blue) for a 56 N push force when gyro noise is added. (For interpretation of the references to color in this figure legend, the reader is referred to the web version of this article.)

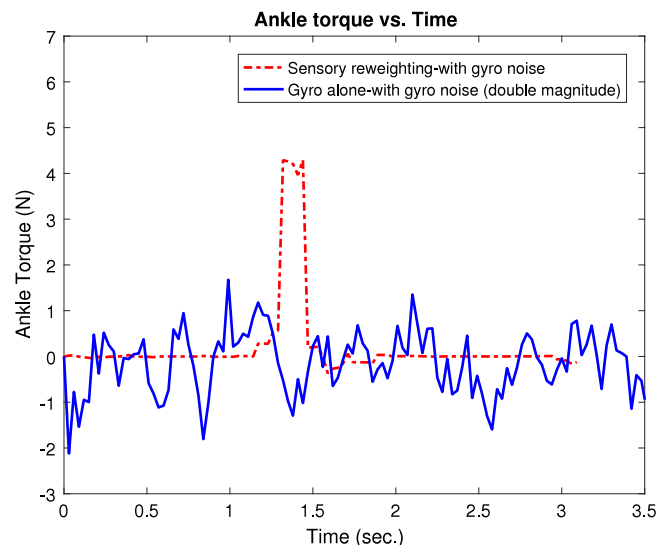


**Fig. 17.** Ankle torque plots using Sensory reweighting (red) and Gyro alone (blue) for a 56 N push force when a double magnitude gyro noise is added. (For interpretation of the references to color in this figure legend, the reader is referred to the web version of this article.)

to Table 2, it is clear that sensory reweighting ensures lower settling time when compared to the same scenario without reweighting. In Scenario 4, the maximum ankle torque applied is 6.44 N while in Scenario 5, the value is 2 N. These values may lead us to think that using gyro alone might be more efficient. However, sensory reweighting applies the torque for a short period of time (just after the push force is applied), but when gyro is used alone the torque is applied during the whole experiment time. This proves, that despite applying a higher torque, the sensory reweighting algorithm proves to be more efficient. The same reasoning applies for the angle displacement, where in some scenarios the maximum angle displacement is higher when using sensory reweighting. The higher angular displacement leads to a faster recovery which is shown in the low settling time in the sensory reweighting scenarios. Therefore, we can conclude that sensory reweighting leads to a faster, more robust, and more efficient humanoid fall avoidance.

When compared to the results in [3], the perturbations applied to Nao are of higher magnitude than the ones in [3]. However, the robot model is of different dimensions and the recovery assessment is of different nature. Also, the push recovery assessment metrics are of a different nature. The metrics used are based on the angle variation per second, while in our approach we measure the impulse force at the moment of impact.

## 9. Conclusions and future work

In this paper, a sensory reweighting algorithm was introduced for a better humanoid fall avoidance performance. The strategy is inspired by human behavior when dealing with everyday disturbances that challenge their balance control. The main idea behind this sensory reweighting algorithm is that operating in different environments requires the integration of different sensors in order

**Table 2**

Performance parameters for the 7 scenarios (maximum torque, maximum displacement angle, and settling time)-Values are averages of the 10 repetitions.

Scenario number	Max. torque (N)	Max. angle displacement (rad)	Settling time (s)
(1) Sensory Reweighting (normal conditions)	1.5	0.33	1.17
(2) Gyro alone (normal conditions)	3.75	0.17	1.95
(3) Camera alone (normal conditions)	2.14	0.42	1.29
(4) Sensory Reweighting (noisy gyro)	6.44	0.39	0.36
(5) Gyro alone (noisy gyro)	2	0.17	1.98
(6) Sensory Reweighting (lights out)	2.24	0.16	2.41
(7) Camera alone (lights out)	0.06	No recovery	No recovery

to diminish the effect of noise. A Kalman Filter is used to reduce the overall estimation error by integrating the visual angle estimation along with the gyroscope's rate estimation. The experimental scenarios described in the previous section demonstrate that the sensory reweighting system performs better in terms of the magnitude of the ankle torque as well as the settling time in the angular displacement. The systems are compared under identical conditions while only changing the variable under test in each case.

For future work, we are considering a more complex humanoid model in order to apply the push recovery algorithm in the frontal plane as well. The ankle strategy alone helps in recovering from small perturbation as mentioned in the literature review. Therefore, our aim is to add the hip and stepping strategy to our system, in order to recover from higher magnitude disturbances. Finally, further study of the human neurological behavior and learning is to be addressed in order to close the gap between human and humanoid push recovery.

## Acknowledgments

This research was funded and supported by AUB University Research Board 2016 and the Lebanese National Council for Scientific Research 2014.

## References

- [1] Onder Tutsoy, CPG based RL algorithm learns to control of a humanoid robot leg, *Int. J. Robot. Autom.* 30 (2) (2015).
- [2] Yoshihiro Kuroki, Masahiro Fujita, Tatsuzo Ishida, Kenichiro Nagasaka, Jin Ichi Yamaguchi, A small biped entertainment robot exploring attractive applications, in: *Robotics and Automation, 2003 Proceedings, ICRA'03, IEEE International Conference on*, vol. 1, IEEE, 2003, pp. 471–476.
- [3] Bassam Jalgha, Daniel Asmar, Imad Elhaji, A hybrid ankle/hip preemptive falling scheme for humanoid robots, in: *Robotics and Automation, ICRA, 2011 IEEE International Conference on*, IEEE, 2011, pp. 1256–1262.
- [4] Takeshi Tanaka, Tomohito Takubo, Kenji Inoue, Tatsuo Arai, Emergent stop for humanoid robots, in: *Intelligent Robots and Systems, 2006 IEEE/RSJ International Conference on*, IEEE, 2006, pp. 3970–3975.
- [5] Marko Nardini, Dorothy Cowie, A.J. Bremner, D.J. Lewkowicz, C. Spence, The development of multisensory balance, locomotion, orientation and navigation, 2012, 137–158.
- [6] R.J. Peterka, Sensorimotor integration in human postural control, *J. Neurophysiol.* 88 (3) (2002) 1097–1118.
- [7] B. Horak Fay, Postural orientation and equilibrium: What do we need to know about neural control of balance to prevent falls?, *Age Ageing* 35 (2) (2006) ii7–ii11.
- [8] A. Tahboub Karim, Biologically-inspired humanoid postural control, *J. Physiol.-Paris* 103 (3) (2009) 195–210.
- [9] A. Winter David, Human balance and posture control during standing and walking, *Gait & Posture* 3 (4) (1995) 193–214.
- [10] Sukyung Park, Fay B. Horak, Arthur D. Kuo, Postural feedback responses scale with biomechanical constraints in human standing, *Exp. Brain Res.* 154 (4) (2004) 417–427.
- [11] Kim Seyoung, Christopher G. Atkeson, Sukyung Park, Perturbation-dependent selection of postural feedback gain and its scaling, *J. Biomech.* 45 (8) (2012) 1379–1386.
- [12] Brian E. Maki, William E. McIlroy, The role of limb movements in maintaining upright stance: the change in support strategy, *Phys. Ther.* 77 (5) (1997) 488–507.
- [13] Oatis Carol, *Kinesiology: The Mechanics and Pathomechanics of Human Movement-0781755131-66, 97, 2004.*
- [14] *Posture: Types Assessment and Control, Illustrated, Nova Science, 2011.*
- [15] Lim Sharon, S.N. Oh, Kwang In Kim, Balance control for biped walking robots using only zero-moment-point position signal, *Electron. Lett.* 48 (1) (2012) 19–20.
- [16] Vukobratovi Miomir, Branislav Borovac, Zero-moment point thirty five years of its life, *Int. J. Humanoid Robot.* 1 (01) (2004) 157–173.
- [17] Mahboobin Arash, Patrick J. Loughlin, Mark S. Redfern, Stuart O. Anderson, Christopher G. Atkeson, Jessica K. Hodgins, Sensory adaptation in human balance control: lessons for biomimetic robotic bipeds, *Neural Netw.* 21 (4) (2008) 621–627.
- [18] T.J. Klein, J. Jeka, T. Kiemel, M.A. Lewis, Navigating sensory conflict in dynamic environments using adaptive state estimation, *Biol. Cybern.* (2012).
- [19] Mohammad-Ali Nikouei Mahani, Shahram Jafari, Hadi Rahmatkhan, A novel approach for humanoid push recovery using stereopsis, *Robotica* 32 (03) (2014) 413–431.
- [20] Onder Tutsoy, Duygun Erol Barkana, Sule Colak, Learning to balance an NAO robot using reinforcement learning with symbolic inverse kinematic, *Trans. Inst. Meas. Control* (2016).
- [21] Colasanto Luca, Nikos G. Tsagarakis, Darwin G. Caldwell, A compact model for the compliant humanoid robot coman, in: *Biomedical Robotics and Biomechanics, BioRob, 2012 4th IEEE RAS & EMBS International Conference on*, IEEE, 2012, pp. 688–694.
- [22] Onder Tutsoy, Duygun Erol Barkana, Sule Colak, Learning to balance an NAO robot using reinforcement learning with symbolic inverse kinematic, *Trans. Inst. Meas. Control* (2016).
- [23] Pratt Jerry, Ambarish Goswami, John Reula, Fabian Canas, Learning capture points for humanoid push recovery, US Patent 8,195,332, issued June 5, 2012.
- [24] Recep, A. Ozdemir, Amir Pourmoghammad, Paloski William H., Sensorimotor posture control in the blind: Superior ankle proprioceptive acuity does not compensate for vision loss, *Gait & Posture* 38 (4) (2013) 603–608.
- [25] Stephan Weiss, Davide Scaramuzza, Roland Siegwart, Monocular-SLAM based navigation for autonomous micro helicopters in GPS-denied environments, *J. Field Robot.* 28.6 (2011) 854–874.
- [26] B.J. Stephens, State estimation for force-controlled humanoid balance using simple models in the presence of modeling error, in: *2011 IEEE International Conference on Robotics and Automation, Shanghai, 2011*, pp. 3994–3999.
- [27] Xinjilefu, C.G. Atkeson, State estimation of a walking humanoid robot, in: *2012 IEEE/RSJ International Conference on Intelligent Robots and Systems, Vilamoura, 2012*, pp. 3693–3699.
- [28] M.F. Fallón, M. Antone, N. Roy, S. Teller, Drift-free humanoid state estimation fusing kinematic, inertial and LIDAR sensing, in: *2014 IEEE-RAS International Conference on Humanoid Robots, Madrid, 2014*, pp. 112–119.
- [29] K. Masuya, T. Sugihara, COM motion estimation of a Humanoid robot based on a fusion of dynamics and kinematics information, in: *2015 IEEE/RSJ International Conference on Intelligent Robots and Systems, IROS, Hamburg, 2015*, pp. 3975–3980.
- [30] Stephens Benjamin, Humanoid push recovery, in: *Humanoid Robots, 2007 7th IEEE-RAS International Conference on*, IEEE, 2007, pp. 589–595.
- [31] Andrew J. Davison, Ian D. Reid, Nicholas D. Molton, Olivier Stasse, MonoSLAM: Real-time single camera SLAM, *IEEE Trans. Pattern Anal. Mach. Intell.* 29 (6) (2007) 1052–1067.

- [32] Frederique Crete, Thierry Dolmiere, Patricia Ladret, Marina Nicolas, The blur effect: perception and estimation with a new no-reference perceptual blur metric, in: In *Electronic Imaging 2007, International Society for Optics and Photonics*, 2007 64920I-64920I.
- [33] Ligorio Gabriele, Angelo Maria Sabatini, Extended Kalman filter-based methods for pose estimation using visual, inertial and magnetic sensors: Comparative analysis and performance evaluation, *Sensors* 13 (2) (2013) 1919–1941.



**Noel Maalouf** received his Bachelor of Engineering degree in Electrical and Computer Engineering, with distinction, from the American University of Beirut, in 2012. In 2013, he was enrolled in the Accelerated Ph.D. program in the same university. He is currently pursuing his Ph.D. in Robotics and Control. He has been working as a Research Assistant in the Computer Vision and Robotics Lab of AUB since 2012.

Noel's research interests include humanoid robotics, bipedal stability, biomimetics, and computer vision. Noel received CNRS-L Doctoral Scholarship Award from the Lebanese National Council for Scientific Research in September 2014.



**Imad H. Elhajj** received his Bachelor of Engineering in Computer and Communications Engineering, with distinction, from the American University of Beirut in 1997 and the M.S. and Ph.D. degrees in Electrical Engineering from Michigan State University in 1999 and 2002, respectively. He is currently an Associate Professor with the Department of Electrical and Computer Engineering at the American University of Beirut.

Dr. Elhajj is the vice-chair of IEEE Lebanon Section, senior member of IEEE and senior member of ACM. He is a member of the World Economic Forum Global Agenda Council on Artificial Intelligence and Robotics. His research interests include instrumentation and robotics, cyber security, sensor and computer networks, and multimedia networking.

Imad received the Most Outstanding Graduate Student Award from the Department of Electrical and Computer Engineering at Michigan State University

in April 2001, the Best Paper award at the IEEE Electro Information Technology Conference in June 2003, and the Best Paper Award at the International Conference on Information Society in the 21st Century in November 2000. Dr. Elhajj is recipient of the Teaching Excellence Award at the American University of Beirut, June 2011 and the Kamal Salibi Academic Freedom Award, 2014.



**Elie Shammass** graduated from the American University of Beirut with a B.E. degree from the Mechanical Engineering Department in 1999. Then under the guidance of Professors Howie Choset and Alfred Rizzi he acquired a project-work Masters of Science and Ph.D. from the Mechanical Engineering Department at Carnegie Mellon University in May 2001 and March 2006, respectively.

From 2007 till 2010, Elie worked as a research and development engineer at Hexagon Metrology where he developed kinematic calibration algorithms for high accuracy portable coordinate measuring machines. Since 2010,

Elie has been an Assistant professor in the Mechanical Engineering Department at the American University of Beirut. Elie's research expertise span multiple disciplines such as robotic joint and mobile robotic platform design, nonholonomic motion planning, and kinematics of robotic manipulators.



**Daniel Asmar** is an Associate Professor in Mechanical Engineering at the American University of Beirut. Daniel received his Bachelors degree in Mechanical Engineering from the University of Waterloo in 1993. He later earned his Masters degree in Mechanical Engineering from the American University of Beirut in 2002, and his Ph.D. in Systems Design Engineering from the University of Waterloo in 2006.

Daniels research interests are in Robotics and Computer Vision. Specifically, he has interests in visual perception, autonomous robot navigation and mapping, environment representation and recognition, and segmentation methods in Computer Vision. He has several publications in these areas in refereed journals and conference proceedings Daniel is a senior member in IEEE and is the advisor of the ASME chapter at AUB. Daniel also has working experience in industry in mechanical and industrial design as well as in construction management.